The power spectrum of $x(n)$ can be efficiently calculated directly form the DHT $H_x(k)$ as[7]

$$|X(k)|^2 = [H_x^2(k) + H_x^2(-k)]/2 \tag{8}$$

Also by eqn. 3, the cepstrum $c_1(n)$ can be computed by the IDFT of $\ln|H_1(k)|$

$$c_1(n) = \frac{1}{N}\sum_{k=0}^{N-1} \ln|H_1(k)|\, e^{j2\pi nk/N} \tag{9}$$

Since the output of the IDFT (the cepstrum) $c_1(n)$ is guaranteed to be real, then the IDFT equals the IDHT, we can obtain $c_1(n)$ from the IDHT of $\ln|H_1(k)|$ as

$$c_1(n) = \frac{1}{N}\sum_{k=0}^{N-1} \ln|H_1(k)|\, \mathrm{cas}\left(\frac{2nk}{N}\pi\right) \tag{10}$$

In summary, the steps necessary to obtain $h_2(n)$ from $h_1(n)$ are

(*a*) Prepare $h_1(n)$ for length N odd (eqn. 1).

(*b*) Take forward FHT of $h_1(n)$ and compute the power spectrum of $h_1(n)$ (eqn. 8).

(*c*) Compute the log magnitude response $\ln|H_1(k)|$.

(*d*) Calculate $c_1(n)$ by taking the IDHT of $\ln|H_1(k)|$ (eqn. 10).

(*e*) Obtain a new sequence $t(n)$ from the recursive formula in eqn. 4.

$$t = 0 \qquad n < 0$$

$$t = h_1(n) \qquad n = 0$$

$$t = c_1(n)t(0) + \sum_{k=0}^{n-1}\frac{k}{n}c_1(n)t(n-k)$$

$$0 \le n \le \frac{N-1}{2} \tag{11}$$

(*f*) Get the scaling factor R for unity in the passband.

$$R = \frac{\sqrt{\left|\sum_{n=0}^{N-1} h_1(n)\right|}}{\sum_{n=0}^{(N-1)/2} t(n)} \tag{12}$$

(*g*) Scale the impulse response $t(n)$

$$h_2(n) = Rt(n) \qquad 0 \le n \le \frac{N-1}{2}$$

The above steps are performed entirely in the real domain and require only two FHT computations. The proposed algorithm has been tested for designing several mininum phase FIR filters. Two short length 256-point real FHTs are sufficient to give satisfactory results equivalent to Reddy's two FFT computations.[6] The differential cepstrum method needs three long 1024-point complex FFTs.[4]

Conclusions: The cepstrum and fast Hartley transform have been used for designing equiripple minimum-phase FIR filters. This fast procedure requires only two short real FHT computations and avoids the complicated phase wrapping and polynomial root-finding algorithms.

S.-C. PEI
S.-B. JAW

Department of Electrical Engineering
National Taiwan University
Taipei, Taiwan, Republic of China

23rd May 1990

References

1 FOXALL, T. G., IBRAHIM, A. A., and HUPE, G. J.: 'Minimum-phase CCD transversal filters', *IEEE Solid-state Circuits*, 1977, **SC-12**, pp. 638–642

2 HERRMANN, O., and SCHUESSLER, H. W.: 'Design of nonrecursive digital filters with minimum-phase', *Electron. Lett.*, 1970, **6**, (11), pp. 329–330

3 MIAN, G. A., and NAINER, A. P.: 'A fast procedure to design equiripple minimum-phase FIR filters', *IEEE Trans.*, 1982, **CAS-29**, pp. 327–331

4 PEI, S. C., and LU, S. T.: 'Design of minimum-phase FIR digital filters by differential cepstrum', *IEEE Trans.*, 1986, **CAS-33**, pp. 570–576

5 REDDY, G. R., and RAO, V. V.: 'On the computation of complex cepstrum through differential cepstrum', *Signal Processing*, 1987, **13**, (1), pp. 79–83

6 REDDY, G. R.: 'Design of minimum-phase FIR digital filter through cepstrum', *Electron. Lett.*, 1986, **22**, (23), pp. 1225–1227

7 BRACEWELL, R. N.: 'The fast Hartley transform', *Proc. IEEE*, 1984, **72**, pp. 1010–1018

8 PEI, S. C., and WU, J. L.: 'Split-radix fast Hartley transform', *Electron. Lett.*, 1986, **22**, (1), pp. 26–27

9 SORENSEN, H. V., JONES, D. L., BURRUS, C. S., and HEIDEMAN, M. T.: 'On computing the discrete Hartley transform', *IEEE Trans.*, 1985, **ASSP-33**, pp. 1231–1238

10 MCCELLAN, J. H., PARKS, T. W., and RABINER, L. R.: 'A computer program for designing optimum FIR linear phase digital filters', *IEEE Trans.*, 1973, **AU-21**, pp. 506–526

HIGH EFFIENCY SMALL-SIZE PLANAR HYPERBOLICAL LENSES

Indexing terms: Integrated optics, Integrated lenses, Focussing

Planar hyperbolical lenses with an average efficiency of 85% for coupling a 40 μm wide beam into a 4 μm wide waveguide are realised. The total length required for the beam compression is 600 μm, with a lateral index contrast of 0·01. Good agreement is found between the BPM predicted and the measured lens efficiencies.

Introduction: Planar lenses are important components for coupling wide beams into narrow waveguides. Miki *et al.*[1] reported geodesical lenses with a focal length of 17 mm and 75% efficiency. Valette *et al.*[2] obtained 60–70% efficiency with Fresnel lenses having a focal length of 8·5 mm. In this letter hyperbolical lenses will be presented combining a 300 μm focal length with efficiencies up to 92% which is the highest for planar lenses so far reported.

Basic principle: Fig. 1 shows the geometry and the ray propagation through a hyperbolical lens. The lens design is based on Fermat's principle which states that in the focal point the optical length $n_1 l_1 + n_2 l_2$ is constant for all ray paths, where l_1 and l_2 are the path lengths in the media with effective refractive indices n_1 and n_2, respectively. The lens shape for aberration-free focusing of a plane wave is thus found to be[3]

$$x^2 = 2fz\left[1 - \frac{n_1}{n_2}\right] + z^2\left[\left(\frac{n_1}{n_2}\right)^2 - 1\right] \tag{1}$$

Lens design and analysis: To determine the optimal lens parameters for coupling a Gaussian beam of width $2w_0$ into a waveguide of width, w_g, we proceeded as follows: The equiva-

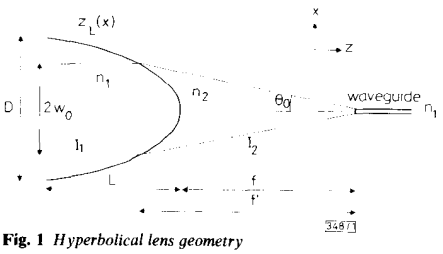

Fig. 1 *Hyperbolical lens geometry*

lent Gaussian width w_m of the waveguide mode was computed from[4]

$$w_m = \frac{w_g}{\sqrt{(2\pi)}}\left(1 + \frac{\sin u}{u} + \frac{1+\cos u}{v}\right) \quad (2)$$

in which u and v are the normalised transverse propagation constants as defined by Unger.[5] In order to obtain a focal width w_m the Gaussian input beam should have a convergence angle θ_0 for which $\sin\theta_0 = \lambda_0/\pi w_m n_2$. The distance f' (see Fig. 1) at which the beam contour (at $1/e^2$ intensity) intersects the lens contour is found from $f' = w_0/tg\theta_0$. The lens parameter f is found by substituting $x = w_0$ and $z = f' - f$ into eqn. 1 and solving the resulting equation for f. We chose a lens diameter D of $4w_0$ (i.e., twice the beam diameter at $1/e^2$ intensity) in order to restrict the spill-over to less than 0.5%. BPM simulations of the hyperbolical lens designed for the theoretical situation described in Table 1 were performed yielding a predicted coupling efficiency to the fundamental mode of the waveguide of 95% (λ_0 was chosen equal to the He-Ne wavelength (633 nm) because of the availability of accurate measurement equipment for this wavelength). The focal point resulting from

Table 1 CHARACTERISTICS OF LENS

	Important properties for the design of the lens				Characteristics of the lens designed for the theoretical situation		
	n_1	n_2	w_g^*	w_{in}^*	f^*	l^*	D^*
Theory	1·573	1·563	4	25	282	323	100
Experiment	1·573	1·562	4	20			

these simulations is in good agreement with the geometrical focal point. BPM simulations were also used to test various methods of segmentation of the lens profile. This segmentation is needed for the realisation of the lens with a pattern generator. Extended information on the lens design (and realisation) is available on request.[6]

Fabrication: To experimentally test the above design we fabricated a set of seven optimal lenses designed for the theoretical situation described in Table 1. Furthermore a set of five lenses was included in which the waveguide-lens distance was varied between 30 μm and 420 μm; a set of three lenses designed for a different waveguide width (2·5 μm, 3 μm and 3·5 μm) and four lenses designed for different contrasts (0·005, 0·007, 0·015, 0·02). Experimental lenses were realised using a $SiO_2/Al_2O_3/SiO_2$ waveguide structure on a silicon substrate. They were fabricated by RF sputter depositing a 0·25 μm Al_2O_3 film ($n \simeq 1{\cdot}69$) onto a thermally oxidised silicon substrate, as described by Smit *et al.*[7] The lateral structure is produced by atom-beam milling a 23 nm step in this layer through a photoresist pattern. The pattern is obtained by projecting an emulsion mask, created by an optical pattern generator (ASET COMBO 250), onto a positive resist film (Hunt Waycoat HPR-204), with a ×4 Canon reduction camera (FPA 141). The etched structure is covered with a 0·6 μm RF-magnetron sputtered SiO_2 layer ($n \simeq 1{\cdot}46$). Fig. 2 shows a photograph of some of the experimental lenses. Up to a distance of 3 μm from the target waveguides the SiO_2 top-layer was chemically etched to a thickness of 0·1 μm and overcoated with a 0·1 μm sputtered Cr layer. This layer was included to absorb light propagating outside the waveguide. This is important for correct detection of the guided power.

Experimental results: Light was coupled in and out of the structure using prism couplers. The efficiency of each lens was determined by measuring the power propagating in the target waveguide and comparing it with the power propagating in the total undiffracted guided wave when the guided wave was excited in the region below the lens (see Fig. 2). The maximum measurement error was estimated to be $\pm 0{\cdot}5$ dB by comparing results of identical lenses. The measured efficiency of the lenses agreed very well with the efficiency predicted by the BPM as can be seen from Fig. 3. The simulation results were

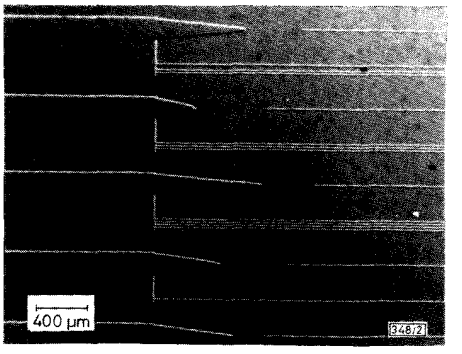

Fig. 2 *Micrograph of part of test structure*
Waveguides between the lenses are used for identification purposes.

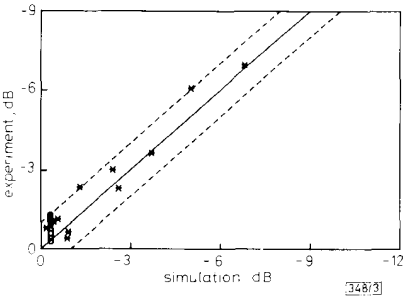

Fig. 3 *Measured and predicted lens efficiencies*
——— ideal case
– – – – 1 dB difference

obtained for the actually realised index contrast of 0·011 instead of the design value 0·01 and for an input beam width of 40 μm instead of 50 μm (see Table 1). The efficiency of the set of seven optimally designed lenses was found to be $84 \pm 8\%$.

Conclusions: Hyperbolical lenses for coupling a 40 μm wide incoming beam into a 4 μm wide waveguide were realised with average efficiencies of 85%. The measured values are in agreement with BPM predictions within 1 dB for predicted losses ranging from −0·3 to −7 dB.

Acknowledgment: We would like to thank Mr. J. W. M. von Uffelen, Mr. A. H. de Vreede of the Technical University of Delft and the staff of the Sensors and Actuators Laboratory of the University of Twente for their help in fabricating and analysing the lenses.

P. C. A. HAMMES
G. J. M. KRIJNEN
A. DRIESSEN
Tramsducers and Materials Science
University of Twente
Faculties of Electrical Engineering and Applied Physics
PO Box 217, 7500 AE Enschede, The Netherlands

M. K. SMIT
Laboratory of Telecommunication and Remote Sensing Technology
Delft University of Technology
Dept. of Electrical Engineering
PO Box 5031, 2600 GA Delft, The Netherlands

7th December 1989

References

1 MIKI, A., OKAMURA, Y., and YAMAMOTO, S.: 'Optical waveguide lens measurement using an image processing system', *Appl. Phys. Lett.*, 1988, **52**, pp. 776–777

2 VALETTE, S., MORQUE, A., and MOTTIER, P.: 'High-performance integrated Fresnel lenses on oxidized Silicon substrate', *Electron Lett.*, 1982, **18**, pp. 13–15
3 BOIVIN, L. P.: 'Thin film laser-to-fiber coupler', *Appl. Opt.*, 1974, **13**, pp. 391–395
4 PASMOOY, W. A., SMIT, M. K., and MANDERSLOOT, P. A.: 'Prism-coupling of light into narrow planar optical waveguides', *J. Lightwave Technol.*, 1989, **LT-7**, pp. 175–180
5 UNGER, H. G.: 'Planar optical waveguides and fibres' (Clarendon Press, Oxford, 1977), Section 2.7
6 HAMMES, P. C. A.: 'Investigation of focusing structures in integrated optics'. Masters Thesis, University of Twente, Enschede, The Netherlands, 1989
7 SMIT, M. K., VAN DER LAAN, C. J., and ACKET, G. A.: 'Aluminium oxide films for integrated optics', *Thin Solid Films*, 1986, **138**, pp. 171–181.

CONTROL OF RADAR CROSS-SECTION AND CROSSPOLARISATION CHARACTERISTICS OF AN ISOTROPIC CHIRAL SPHERE

Indexing terms: Chiral medium, Radar, Radar antennas, Cross-polarisation

With a proper choice of parameters, it may be possible to use a chiral sphere as a polarisation transformer. The key equations describing the scattering properties of the sphere are presented.

The study of chiral media as waveguides,[1,2] antennas[3–5] and scatterers[6,7] at sub-optical frequencies has attracted the attention of researchers for some time. Chirality, or handedness, refers to a lack of bilateral symmetry of an object, e.g., in organic polymers, helices and irregular tetrahedra. Although many studies have appeared in recent years on the basic formulations of some electromagnetic chiral problems, a lot of work remains to be done to determine the suitability of chiral materials for practical use in radar targets, antennas, microwave and millimeter-wave circuits.

Electromagnetic scattering by a chiral sphere has been well documented.[6,7] However, little has been published on whether and how the chiral properties can be used to control the copolarisation and cross polarisation scattering characteristics of the spherical scatterer.

The aim of this letter is to examine the role of chiral parameters in the control of the RCS of the chiral sphere.

We present below the key mathematical equations describing the scattering properties of the sphere. The far zone scattering matrix $\boldsymbol{S}^c$ is given by[5,7]

$$\boldsymbol{S}^c = \begin{bmatrix} S_{11}^c & S_{12}^c \\ S_{21}^c & S_{22}^c \end{bmatrix} \tag{1}$$

where the coefficients are[5,7]

$$S_{11}^c = \sum_{n=1}^{\infty} \frac{2n+1}{n(n+1)} (-a_n \pi_n - b_n \tau_n) \tag{2a}$$

$$S_{12}^c = \sum_{n=1}^{\infty} \frac{2n+1}{n(n+1)} (c_n \pi_n - d_n \tau_n) \tag{2b}$$

$$S_{21}^c = \sum_{n=1}^{\infty} \frac{2n+1}{n(n+1)} (d_n \pi_n - c_n \tau_n) \tag{2c}$$

$$S_{22}^c = \sum_{n=1}^{\infty} \frac{2n+1}{n(n+1)} (-a_n \tau_n - b_n \pi_n) \tag{2d}$$

$$\pi_n = P_n^1(\cos\theta)/\sin\theta \qquad \tau_n = \frac{dP_n^1(\cos\theta)}{d\theta} \tag{3}$$

n is the mode number; the expressions for a_n, b_n, c_n, d_n and other necessary parameters are available in Reference 7. The chiral constants α and β, along with the dielectric constant ε and permeability μ, are given by the constitutive relations

$$\bar{D} = \varepsilon\bar{E} + \alpha\varepsilon\nabla \times \bar{E}$$

and

$$\bar{B} = \mu\bar{H} + \beta\mu\nabla \times \bar{H} \tag{4}$$

The LC and RC wave numbers are

$$k_{L,R} = \omega(\mu\varepsilon)^{1/2}\left\{\frac{1 + (\alpha-\beta)^2\varepsilon\mu\omega^2/4 \pm (\alpha+\beta)\omega(\mu\varepsilon)^{1/2}}{1 - \alpha\beta\mu\varepsilon\omega^2}\right\} \tag{5}$$

For achiral media, $\alpha = \beta = 0$ and $k_{L,R}$ reduces to plane-wave propagation in the host medium and the constitutive relations reduce to those of an achiral medium. It is interesting to note from eqns. 2 that, for a chiral sphere (in fact, for any chiral case) $S_{12}^c \neq S_{21}^c$, and both of them are nonzero. For an achiral medium, $S_{12} = S_{21} = 0$. Eqns. 1 and 2 refer to a left-handed and right-handed circular polarisation.

A computer program has been developed in FORTRAN to study the control of RCS of the chiral sphere using chiral properties. The number of modes to be considered in the infinite series in eqns. 2 is assumed to be of the order of ka, where k is the wave number in the achiral host medium having the same μ and ε.

Fig. 1 shows the plot of $20 \log_{10}|S_{ij}^c|$ with the aspect angle for a chiral sphere of radius λ, $\mu_r = 1$, $\varepsilon_r = 4$ and with $\alpha = 0{\cdot}003$, $\beta = 0{\cdot}002$. Fig. 2 shows the co- and cross-polarisation scattered patterns of the same sphere when it is achiral ($\alpha = \beta = 0$). An examination of Figs. 1 and 2 leads to the following observations: (*a*) the scattering properties of the chiral sphere are aspect-dependent; (*b*) the cross-polarisation components can be considerable for a chiral scatterer; (*c*) there could be a significant difference in the coplanar cross section with $i = j = 1$ and $i = j = 2$ for a chiral sphere, whereas for an achiral sphere they are the same. Hence, as far as crosspolarisation scattering is concerned, a chiral sphere

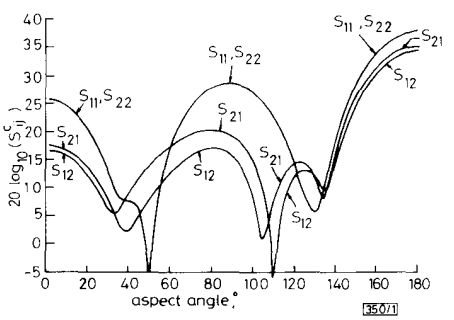

Fig. 1 *Variation of 20 $\log_{10}(|S_{ij}^c|)$ with aspect angle for a chiral sphere of radius λ*

$\mu_r = 1$; $\varepsilon_r = 4$; $\alpha = 0{\cdot}003$; $\beta = 0{\cdot}002$

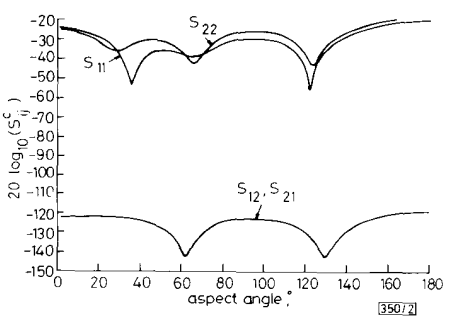

Fig. 2 *Variation of 20 $\log_{10}(|S_{ij}^c|)$ with aspect angle for achiral sphere of radius λ*

$\mu_r = 1$; $\varepsilon_r = 4$; $\alpha = \beta$